JACS
JOURNAL OF THE AMERICAN CHEMICAL SOCIETY
Article
pubs.acs.org/JACS

Scalable and Effective Enrichment of Semiconducting Single-Walled Carbon Nanotubes by a Dual Selective Naphthalene-Based Azo Dispersant

Ashok Kumar Sundramoorthy,[†] Sara Mesgari,[†] Jing Wang,[†] Raj Kumar,[‡] Mahasin Alam Sk.,[†] Siew Hooi Yeap,[†] Qing Zhang,[‡] Siu Kwan Sze,[§] Kok Hwa Lim,*[,†] and Mary B. Chan-Park*[,†]

[†]School of Chemical and Biomedical Engineering, Nanyang Technological University, Singapore 637459, Singapore

[‡]Microelectronics Center, School of Electrical and Electronic Engineering, Nanyang Technological University, Singapore 639798, Singapore

[§]School of Biological Sciences, Nanyang Technological University, Singapore 639798, Singapore

Supporting Information

ABSTRACT: Semiconducting single-walled carbon nanotubes (s-SWNTs) have emerged as a promising class of electronic materials, but the metallic (m)-SWNTs present in all as-synthesized nanotube samples must be removed for many applications. A high selectivity and high yield separation method has remained elusive. A separation process based on selective chemistry appears to be an attractive route since it is usually relatively simple, but more effective chemicals are needed. Here we demonstrate the first example of a new class of dual selective compounds based on polycyclic aromatic azo compounds, specifically Direct Blue 71 (**I**), for high-purity separation of s-SWNTs at high yield. Highly enriched (~93% purity) s-SWNTs are produced through the simple process of standing arc-discharge SWNTs with **I** followed by centrifugation. The s-SWNTs total yield is up to 41%, the highest yet reported for a solution-based separation technique that demonstrates applicability in actual transistors. 91% of transistor devices fabricated with these s-SWNTs exhibited on/off ratios of 10^3 to 10^5 with the best devices showing mobility as high as 21.8 cm^2/V s with on/off ratio of 10^4. Raman and X-ray photoelectron spectroscopic shifts and ultraviolet−visible−near-infrared (UV−vis−NIR) show that **I** preferentially complexes with s-SWNTs and preferentially suspends them. Preferential reaction of naphthyl radicals (generated from **I** with ultrasonication) with m-SWNTs is confirmed by changes in the D-band in the Raman spectroscopy, matrix-assisted desorption−ionization time-of-flight mass spectrometry (MALDI-TOF-MS), and molecular simulation results. The high selectivity of **I** stems from its unique dual action as both a selective dispersion agent and the generator of radicals which preferentially attack unwanted metallic species.

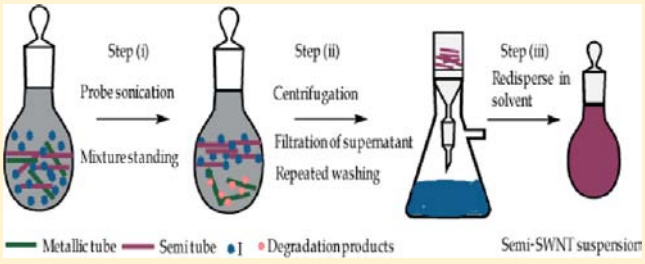

INTRODUCTION

Semiconducting single-walled carbon nanotubes (s-SWNTs) are thought to be a strong contender for the next generation high-performance printable semiconductor which may revolutionize consumer, medical, and macro-electronics.[1−4] However, all current SWNT syntheses, such as carbon-arc discharge, laser ablation of carbon, and chemical vapor deposition methods, produce s-SWNTs which are comingled with metallic (m-) SWNTs.[5] The metallic species contribute unwanted conductance when the nanotubes are applied in transistors and electronic circuits. For high-performance electronic device applications, it is necessary to extract or enrich pure s-SWNTs.[6−12] In recent years, several impressive pre- and postsynthesis approaches to enrich s-SWNTs from as-synthesized nanotube powders have been reported.[9,13−33] However, due to the only subtle differences in the properties of m-SWNTs and s-SWNTs, these methods typically do not achieve sufficiently high purity needed for practical transistors or they entail a trade-off between yield and purity. The lack of a method for low-cost and high volume preparation of high purity s-SWNT samples remains a significant obstacle to the widespread application of s-SWNTs in electronics.[4]

Selective chemistry involving preferential noncovalent adsorption on semiconducting nanotubes or covalent attack of metallic nanotubes seems particularly appealing as the associated separation process is usually rather simple. Various functionalized polycyclic aromatic molecules such as pyrene and naphthalene have shown selectivity for the suspension of s-SWNTs.[13,16,19,30] However, the selectivity of these aromatic compounds, which is based on noncovalent interactions, is generally poor, and also the environment effect (e.g., solvent) and mechanism appear to be not well understood.[34] Schmidt et al. and Strano et al. showed that some water-soluble diazonium compounds, e.g. 4-chlorobenzene diazonium salt, can preferentially extract electrons from m-SWNTs rather than s-SWNTs

Received: March 23, 2012
Published: March 22, 2013

   dx.doi.org/10.1021/ja312282g | J. Am. Chem. Soc. 2013, 135, 5569−5581

to form covalent aryl bonds.[21,22,25] However, the selectivity is generally hard to control and is limited to smaller diameter nanotubes as benzene diazonium salts are unstable and aggressive; control of the concentration of the intermediate reacting species which is speculated to be radicals or cations is typically challenging. We have also demonstrated some m-SWNTs selectivity with other radical forming compounds.[35−38] The selectivity is usually difficult to control and limited to smaller diameter (<1.0 nm CoMoCAT) nanotubes which already have higher s-SWNTs content. We postulate that these previously reported radicals or reactive species are too aggressive. It appears that one of the key challenges in m-SWNT selective attack is the control of the concentration and reactivity of the reacting intermediates, which are usually radicals. Radicals attack both metallic and semiconducting SWNTs although they have some preferential selectivity for m-SWNTs.[35,37,39] If the radical concentration was limiting and the reactivity controlled, we hypothesize that radical attack would be more restricted to m-SWNTs and the resulting process would be more highly selective. This suggests an approach to the refinement of chemical selection to achieve the high separation purity needed for electronic applications, particularly for larger diameter nanotubes which typically have higher mobility.[40,41]

In this study, we report a facile high yield route to obtain highly enriched s-SWNTs solution by using a sulfonate-functionalized naphthalene-based azo compound, specifically the dye direct blue 71 (**I**), (i.e., 1,5-naphthalenedisulfonic acid, 3-[[4-[[4-[(6-amino-1-hydroxy-3-sulfo-2-naphthyl)azo]-6-sulfo-1-naphthyl]azo]-1-naphthyl] azo]-, tetra sodium salt) (Figure 1a). This compound is uniquely doubly selectively—

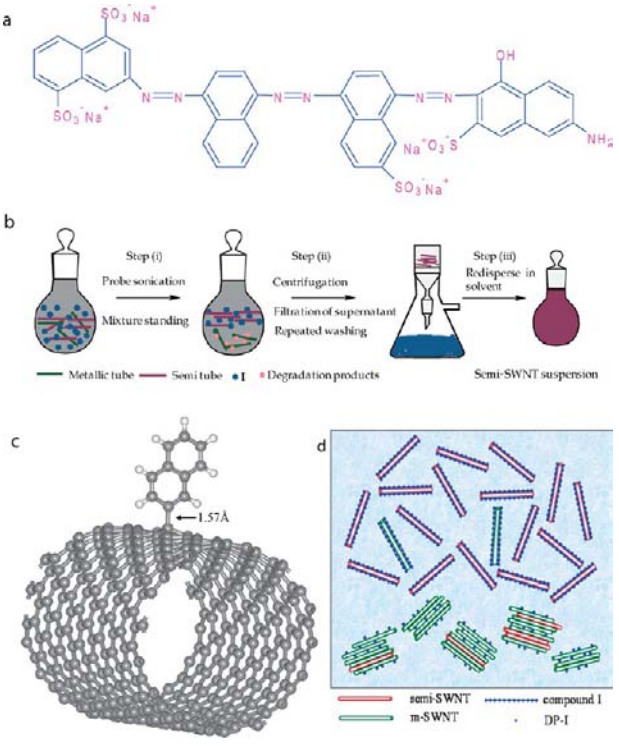

Figure 1. (a) Chemical structure of **I**. (b) Schematic representation of semiconducting SWNT separation using **I**. (c) Optimized complex structure of 2-naphthyl radical and m-SWNT (15,3). Gray sphere − C atom and white sphere − H atom. (d) Schematic separation mechanism with **I**.

the undecomposed **I** selectively suspends s-SWNTs, but it slowly decomposes to form relatively stable naphthyl-based radicals in limiting quantities that preferentially attack m-SWNTs; hybrids formed by the reaction of degradation products (DP) of **I** with m-SWNTs are denser than unreacted s-SWNTs and settle under centrifugation. Unlike previous chemicals, naphthalene-based azo compounds are relatively stable but also form relatively stable radicals at controllable low concentrations with sonication, heat, standing, and so forth.[22] The radicals generated from **I** are more stabilized by the resonance effect of the larger naphthalene groups, than are the benzyl, phenyl or aliphatic radicals produced by previously reported chemicals. Further, our proposed agent **I** in its active undecomposed state is hypothesized to be a s-SWNT selective dispersant. Naphthalene groups, like other large aromatics, are somewhat selective for s-SWNTs, but this effect is highly accentuated in **I** since each molecule has four naphthalene groups together with four ionic sulfonate groups. The sulfonate groups, which are electron withdrawing and ionic, improve the s-SWNTs selectivity and confer dispersing power. Unlike previous selective chemicals used, **I** itself is an effective dispersing agent so that no other dispersant/surfactant is needed in the solvation cum selection process.

Selective enrichment of s-SWNTs is achievable by simply (a) mixing purified arc-discharge P2-SWNTs with direct blue 71 (**I**) with heating and sonication, (b) letting the mixture stand for few days, and then (c) centrifugation to obtain enriched s-SWNTs in the supernatant (Supt) (Figure 1b). Hereinafter, the solids which remain suspended after centrifugation are called Supt-SWNTs, while the precipitate is called Ppt-SWNTs. UV−visible−near infrared (UV−vis−NIR) spectroscopy and Raman spectroscopy were performed on the separated fractions. UV−vis−NIR spectroscopy and Raman spectroscopy show the Supt-SWNTs to be s-SWNTs enriched and the Ppt-SWNTs to be m-SWNTs enriched. UV−vis−NIR shows the purity and yield of s-SWNTs extracted with one pass standing/centrifugation to be 93% and up to 41%, respectively. The selective suspension of s-SWNTs in Supt-SWNTs was also confirmed with high performance switchable field effect transistors (FETs). Spectroscopic shifts observed in Raman spectroscopy and X-ray photoelectron spectroscopy (XPS) suggest that undecomposed **I** interacts preferentially with suspended s-SWNTs. Matrix-assisted laser desorption/ionization coupled with time of flight mass spectrometry (MALDI-TOF-MS) and density functional calculations confirm that the degradation products (DP) of **I**, which are likely to be naphthyl-based radicals, preferentially react with m-SWNTs. The reacted products of DP-**I** and m-SWNTs, which have higher masses than the mostly unreacted s-SWNTs, settle under centrifugation. Further, replacement of centrifugation in step (ii) in Figure 1b with density gradient ultracentrifugation (DGU) with a single surfactant, sodium cholate (Supplementary Figure S1), produces 98% ultrapure s-SWNTs. Depending on the details of the density separation step, **I** may be used to prepare high purity s-SWNTs with high yield or ultrahigh purity s-SWNTs with lower yield.

■ RESULTS AND DISCUSSION

UV−vis−NIR spectroscopy has been reported to be an important tool for characterizing the metallicity of SWNTs.[42] Figure 2a shows the UV−vis−NIR absorption spectra of (i) Pristine P2-SWNTs, (ii) separated Supt-SWNTs (predominantly s-SWNTs), and (iii) Ppt-SWNTs (significantly enriched

dx.doi.org/10.1021/ja312282g | J. Am. Chem. Soc. 2013, 135, 5569−5581

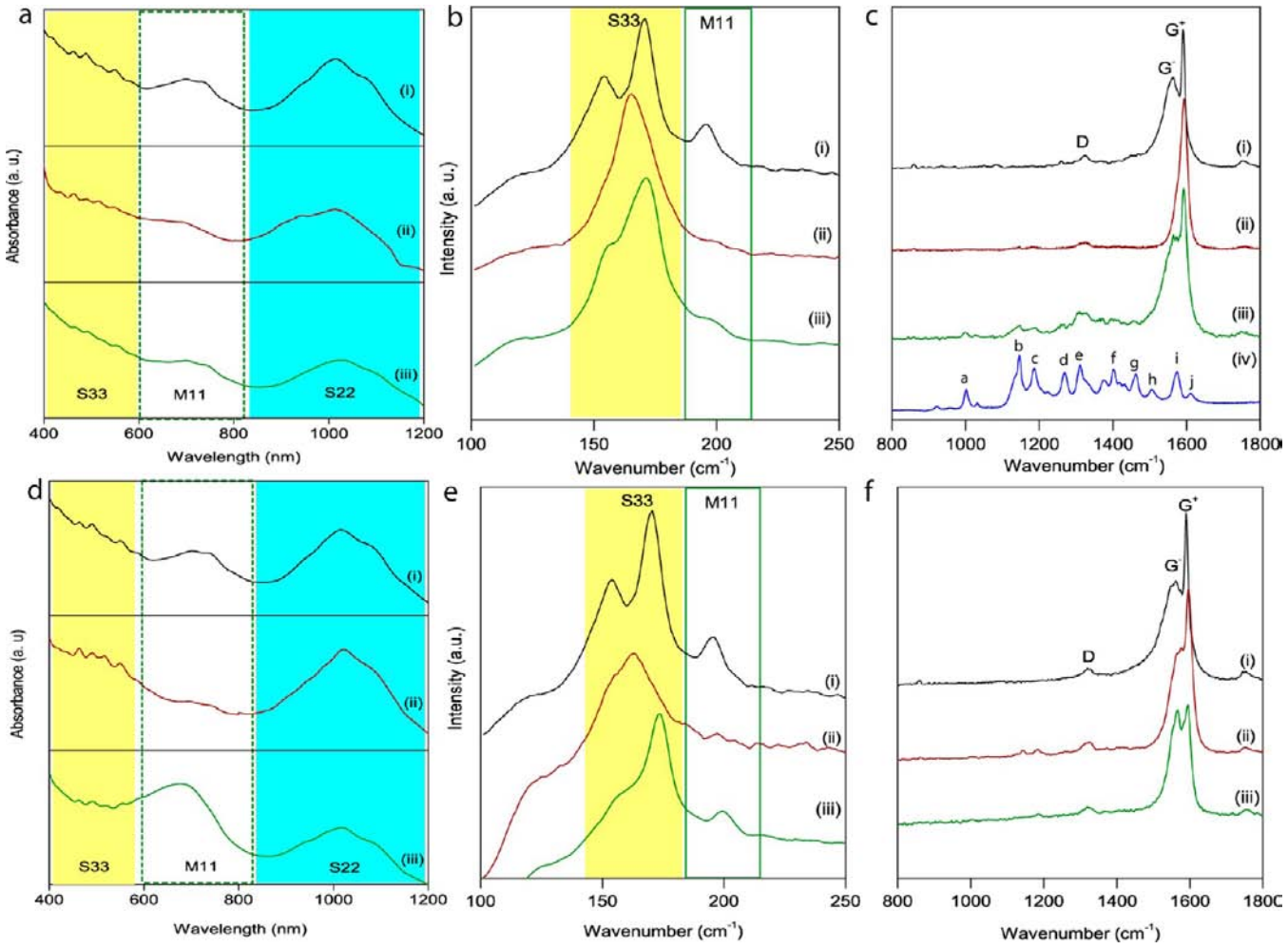

Figure 2. (a–c) SWNT (P2) samples treated with **I** and centrifugation. (i) Pristine P2-SWNTs (control), (ii) separated Supt s-SWNTs, and (iii) separated Ppt-SWNTs and (iv) dye **I**. (a) UV–vis–NIR spectra; (b, c) Raman spectra of SWNTs samples with centrifugation; (d–f) SWNT fractions after treatment with **I** and DGU. (i) Pristine P2-SWNT (control), (ii) separated pink fraction enriched in s-SWNTs, and (iii) separated green fraction enriched in m-SWNTs. (d) UV–vis–NIR spectra; (e, f) Raman spectra of **I** treated SWNTs samples with DGU; (i) Pristine P2-SWNT (control), (ii) separated s-SWNT, and (iii) m-SWNT.

in m-SWNTs), all dispersed in a 1% cosurfactant SDS/SC (1:4) solution. The first interband transition for metallic tubes, M_{11} (peak at 719 nm), and the third and second interband transitions for semiconducting tubes, S_{33} (460–488 nm) and S_{22} (920–1120 nm), are indicated. For the Supt-SWNTs sample (Figure 2a, curve ii), the peak corresponding to the metallic band (M_{11}) is suppressed. It has been reported that the S_{22} peak in the UV–vis–NIR spectra can be used for purity evaluation because it is less affected by doping during chemical purification than is the S_{33} peak.[43] Accordingly, the purity of the various fractions was estimated through comparison of the M_{11} and S_{22} peak areas of the respective spectra. In the separated Supt-SWNT suspension, the semiconducting SWNT purity was evaluated to be 93%, compared with 82% for pristine P2-SWNTs (See Supplementary Figures S2A and S2B). Hence, the Supt-SWNTs sample is enriched in s-SWNTs with respect to m-SWNTs. Based on the measured weight after the separation, the average yield of s-SWNTs in the Supt-SWNTs fraction was estimated to be up to 41% of the original P2-SWNTs semiconducting species content (Supplementary Table S1). This is an unprecedented high yield of high purity s-SWNTs achieved with a very simple separation procedure. For the Ppt-SWNTs sample (Figure 2a, curve iii), the M_{11} metallic band appears to be suppressed because of selective reaction of the radical to the metallic nanotubes; this has been observed by Kim et al.[44] and Mevellec et al.[45] for the diazonium chemistry.

Raman spectroscopy has been extensively used to investigate the electronic and vibrational properties of SWNTs.[46] To evaluate the separation of s-SWNTs, Raman spectra were recorded using a helium–neon laser (633 nm), which resonantly probes both m- and s-arc discharge SWNTs. It should be noted that the single laser wavelength used only allows detection of some diameter species present, but the 633 nm laser is useful for characterizing arc discharge SWNTs with the diameter range of 1.32–1.72 nm.[47−52] Figure 2b displays the Raman spectra in the radial breathing mode (RBM) range of (i) pristine, (ii) separated Supt-SWNT, and (iii) separated Ppt-SWNT samples. The lower frequency RBMs (135–180 cm^{-1}, S_{33}) can be attributed to semiconducting nanotubes with diameters calculated to be ∼1.54 nm, due probably to the species (20, 0), a zigzag tube, and/or (12, 11) or (16, 6), which are chiral tubes. The pristine sample (Figure 2b, i) also shows higher frequency RBMs (183–210 cm^{-1}, M_{11}) which can be attributed to metallic nanotubes with average diameter of 1.32 nm, possibly a (16, 1) or a (15, 3) chiral tube. Comparison of the spectrum of the Supt-SWNT sample (Figure 2b, ii) with the

dx.doi.org/10.1021/ja312282g | J. Am. Chem. Soc. 2013, 135, 5569–5581

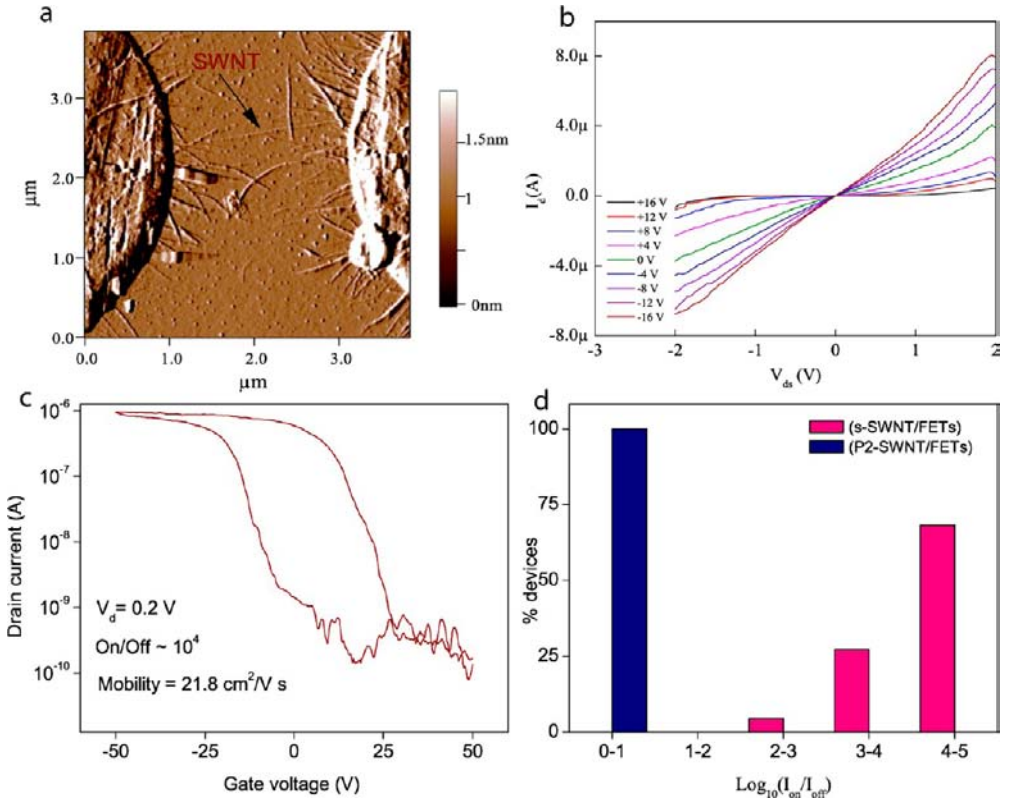

Figure 3. Using sorted P2 samples (a), AFM image of a bridged s-SWNT field-effect transistor. (b) Output curves of an as-prepared s-SWNT-FET as a function of gate voltages from +16 to −16 V in steps of 4 V. (c) Transfer characteristics of a typical s-SWNT FET device at V_{ds} = 0.2 V. (d) Histogram of on/off ratios of fabricated FET devices made with Supt s-SWNTs (red) and pristine P2-SWNTs (control sample-blue).

pristine nanotubes (Figure 2b, i) indicates that the higher frequency RBMs (183−210 cm^{-1}, M_{11}) are absent from the former, confirming that metallic species are highly depleted from the Supt-SWNT fraction, which is essentially a s-SWNT enriched solution. For the Ppt-SWNT (Figure 2b, curve iii), the M_{11} RBM peak is present but attenuated in intensity as the metallic nanotubes have been covalently modified; earlier reports by Mevellec et al. have also observed the suppression of RBM (M_{11}) peak after the covalent functionalization.[45,53] (This shall be further elaborated below.)

The Raman signatures in the frequency range between 1450 and 1700 cm^{-1} (Figure 2c) show the nanotube tangential modes with the characteristic G^+ and G^- features. For the pristine sample (Figure 2c, i), the G^- mode (at 1563 cm^{-1}) is broad and asymmetrical with a Breit−Wigner−Fano profile because of phonon−-plasmon coupling with a continuum of states present only in metallic nanotubes. The G^- band area in the Supt-SWNT sample (Figure 2c, curve ii) is significantly smaller than that of pristine SWNTs (Figure 2c, curve i), corroborating the RBM mode data that metallic nanotube content is diminished in Supt-SWNTs. In contrast, the Ppt-SWNTs (Figure 2c, iii) sample shows a strong G^- band, corroborating that this fraction contains significant m-SWNT content (Figure 2c).

The compound **I** also shows its own characteristic Raman peaks (Figure 2c, curve iv, peaks a to j and Table S2). From the Raman spectrum of Supt-SWNTs (Figure 2c, curve ii), we found that the Raman peaks of **I** almost disappeared from the Supt-SWNTs after repeated washing with distilled water and dimethylformamide (DMF) solvent. In contrast, some peaks of **I**, but not all of the **I** peaks, and a significant disorder (D) band were observed in the Raman spectrum of Ppt-SWNT (Figure 2c, curve iii), corroborating that the Ppt-SWNTs are selectively covalently attacked by **I**/DP-**I** which are not removable.

Density-gradient ultracentrifugation (DGU) is a standard sorting technique that allows SWNTs to be separated by their buoyant density in a surfactant solution.[14] We expect a buoyancy contrast between m-SWNTs and s-SWNTs after treatment with **I**. We employed DGU to separate **I**-treated SWNTs dispersed in a surfactant solution (1% SC). After the DGU, three different colored layers were identified (Supplementary Figure S1), and the two upper suspended layers were carefully extracted (without mixing) using a micro syringe, stored in separate glass vials and characterized with UV−vis−NIR and Raman spectroscopies. We identified the pink fraction to be s-SWNTs and the green fraction to be m-SWNTs (Figure 2d). We estimated the purity of the s-SWNTs as described previously and found it to be 98.1% (Supplementary Figure S3). (In a control experiment, we used pristine P2-SWNTs dispersed in 1% SC to separate SWNTs by DGU. As shown in Supplementary Figure S1, SWNT separation by metallicity is not achieved without **I** treatment). For the pink fraction, the RBM region of the Raman spectrum (Figure 2e, curve ii) is visibly devoid of the M_{11} peak, confirming the pink fraction to be s-SWNTs enriched. For the same pink fraction, the metallic G^- peak is also significantly diminished (Figure 2f, curve ii). For the green fraction, the metallic G^- peak (Figure 2f, curve iii) is much enhanced with respect to the pink fraction (ii), indicating enrichment of m-SWNTs in this fraction. Also, a strong M_{11} RBM peak is observed in the Raman spectrum of the green fraction which further demonstrates enrichment of m-SWNTs in the suspended green fraction. The buoyant

dx.doi.org/10.1021/ja312282g | J. Am. Chem. Soc. 2013, 135, 5569−5581

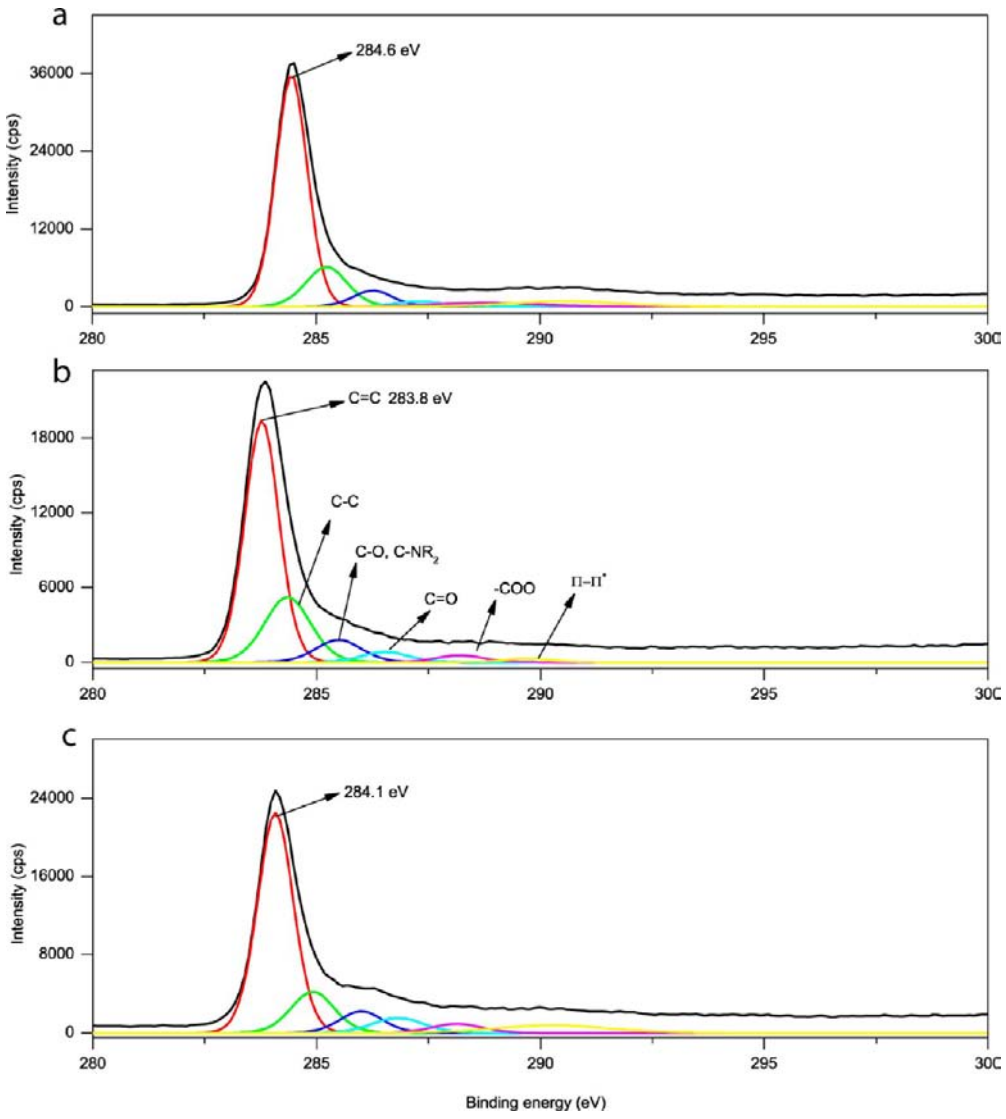

Figure 4. XPS high resolution C1s peak deconvolution data (using P2 nanotubes). (a) Pristine-P2-SWNTs (control). (b) Supt-SWNTs and (c) Ppt-SWNTs and the assigned bonds. (Normalized to Au 4f7 peak at 84.0 eV as internal standards).

densities of pink (semi enriched) and green (metallic enriched) layers were determined to be 1.07 g/cm^3 and 1.13 g/cm^3 from their positions in the density gradient profile shown in the Supplementary Figure S4.[14,54] This study shows that very high semiconducting purity SWNTs may be produced with **I** standing and DGU, but the yield is lower than that achieved by the regular centrifugation method described earlier, and all further experiments and analysis reported below focus on the SWNT fractions separated by the high-*s*-yield regular centrifugation method.

A further test for enrichment of s-SWNTs, or depletion of m-SWNTs, in Supt-SWNTs (without DGU) is the performance of field effect transistors (FETs) which employ enriched Supt-SWNTs as the active material. This kind of device is in demand for flexible electronics and sensors.[55] We fabricated FET devices (on 300 nm SiO_2 gate oxide layer on Si wafer) by depositing/orienting s-SWNTs in the FET channel through alternating current (ac-) dielectrophoresis method (Supplementary Figure S5). Atomic force microscopy (AFM) imaging of the devices showed that few single nanotubes bridged the source and drain electrodes (Figure 3a). The s-SWNT tubes appeared to be relatively straight and aligned parallel to one another. The resistance of the s-SWNT devices was approximately 3−4 MΩ, which is higher than the resistance of other reported SWNT field effect transistors prepared by AC dielectrophoresis method, which were prepared with unseparated nanotube samples containing metallic nanotubes.[56−58] The higher resistance of our devices suggests that the aligned tubes on the channel are significantly depleted in m-SWNTs. As shown in Figure 3b, FETs based on the as-separated s-SWNTs show a typical p-type field effect characteristic of s-SWNTs in ambient conditions, with the drain current increasing with increasing negative gate voltage. In Figure 3c, we show the transfer characteristics of a back-gated s-SWNT device. The as-prepared device is a p-type FET with $I_{on} \sim 1\ \mu A$, and the threshold slope is 1000 mV/decade. We investigated more than 25 FET devices and found the on/off ratios to range from about 10^2 to about 10^5, with the distribution weighted toward the high end of this range. Figure 3d shows the distribution of ON/OFF ratios for s-SWNT/FET devices prepared from our separated Supt s-SWNT solution. For comparison, devices prepared with the same procedure using

dx.doi.org/10.1021/ja312282g | *J. Am. Chem. Soc.* 2013, 135, 5569−5581

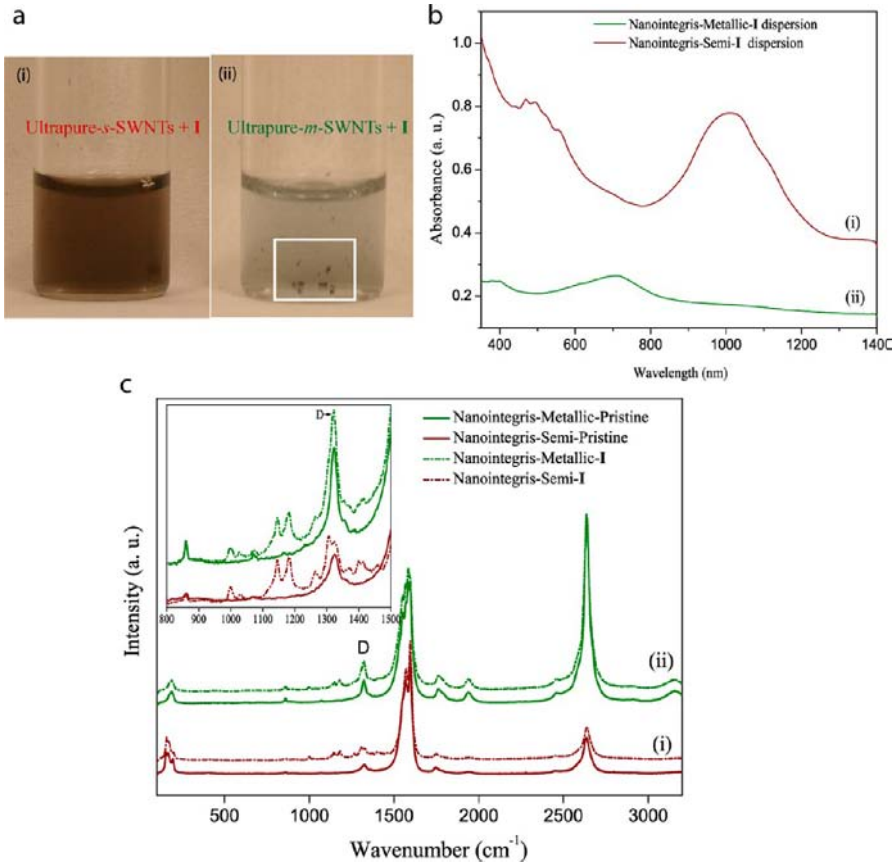

Figure 5. Dispersion using ultrapure semi/metallic SWNTs purchased from NanoIntgeris, IL, USA (a) and (b) dispersion of ultrapure semiconducting and metallic nanotubes from NanoIntegris suspended with dye **I**. (a) Photographic images of (i) ultrapure semi- (99%) and (ii) metallic nanotubes (99%) powders (surfactant-free) dispersed in **I**/water solution (without any other surfactant) and (b) corresponding UV−vis−NIR spectra of ultrapure-s-SWNTs (curve i) and m-SWNTs (curve ii) dispersion in **I**/water. (c) Raman spectra (633 nm) of ultrapure-metallic SWNTs (99%) and semiconducting SWNT powders (surfactant free) (99%) before and after treatment with **I**.

pristine P2-SWNT solution are also shown. The devices made with unseparated SWNTs all have ON/OFF ratios less than 10. The best device using the s-SWNTs exhibits an estimated hole mobility of 21.8 cm^2 /V s with on/off ratio of 10^4 (Figure 3c). Our method is a simple and convenient way to provide the s-SWNTs necessary for high performance solution processable SWNT-FET devices. This is the first report of larger diameter s-SWNTs purified by chemical separation technique that demonstrate good FETs.

We postulate that there is preferential molecular charge transfer between undecomposed **I** and the s-SWNTs. High-resolution X-ray spectroscopy was also performed to study the preferential doping of **I** for s-SWNTs. Figure 4 shows the high-resolution C1s peak of the three samples (the bond type deconvolutions are listed in Supplementary Table S3); the peaks in Figure 4 have all been normalized to Au 4f7 peak at 84.0 eV as internal standard. There is some downshift in the C1s peak of C═C bond of the Supt-SWNTs and Ppt-SWNTs samples compared with the pristine sample, corroborating the phenomenon of charge transfer between the nanotubes and the undecomposed **I**. The downshift of the main sp2 peak is more severe in Supt-SWNTs than in Ppt-SWNTs, corroborating that the charge transfer interaction is stronger with Supt-SWNTs than with Ppt-SWNTs. The stronger interaction between s-SWNTs and undecomposed **I** is also evident from the upshift by 1.8 cm^{-1} of the Raman G^+ peak of the Supt-s-SWNTs sample compared with the pristine sample (Supplementary Figure S6).[52] The Ppt-SWNTs sample does not show any upshift. The Raman upshift can be attributed to charge transfer from SWNTs to electron-withdrawing sulfonate group-functionalized naphthalene.

The selective suspension of s-SWNTs by **I** was also investigated by additional experiments carried out with ultrapure metallic (99%) and semiconducting nanotubes (99%) (surfactant-free powders purchased from NanoIntgeris, IL, USA). (Only Figure 5 needed for mechanistic study was done with a different type of nanotubes—ultrapure s- or m-SWNTs from NanoIntegris, as opposed to P2-SWNTs used for all other data.) Equal amounts of pure-metallic and s-SWNTs were separately weighed and dispersed in **I**/water solution by ultrasonication for 1 h. The UV−vis−NIR spectra of solutions of ultrapure s-SWNTs and ultrametallic-SWNTs with **I** were then collected (see Supplementary Experimental Section A for details). Visual observations show particles in the m-SWNTs/**I** solution (Figure 5a, right bottle) but complete dissolution in the s-SWNTs/**I** solution (Figure 5a, left bottle). UV−vis−NIR indicates that the s-SWNTs/**I** solution has higher absorbance than the metallic nanotubes/**I** solution (Figure 5b). Application of Beer's law with Figure 5b shows that the solubility of s-SWNTs in **I**/water (14.88 mg/L) was calculated to be about four times higher than that of metallic SWNTs in **I** (4.03 mg/L).

Further, **I** is a type of azo compound which is generally stable but can generate under ultrasonication or thermal stimulation,

dx.doi.org/10.1021/ja312282g | J. Am. Chem. Soc. 2013, 135, 5569−5581

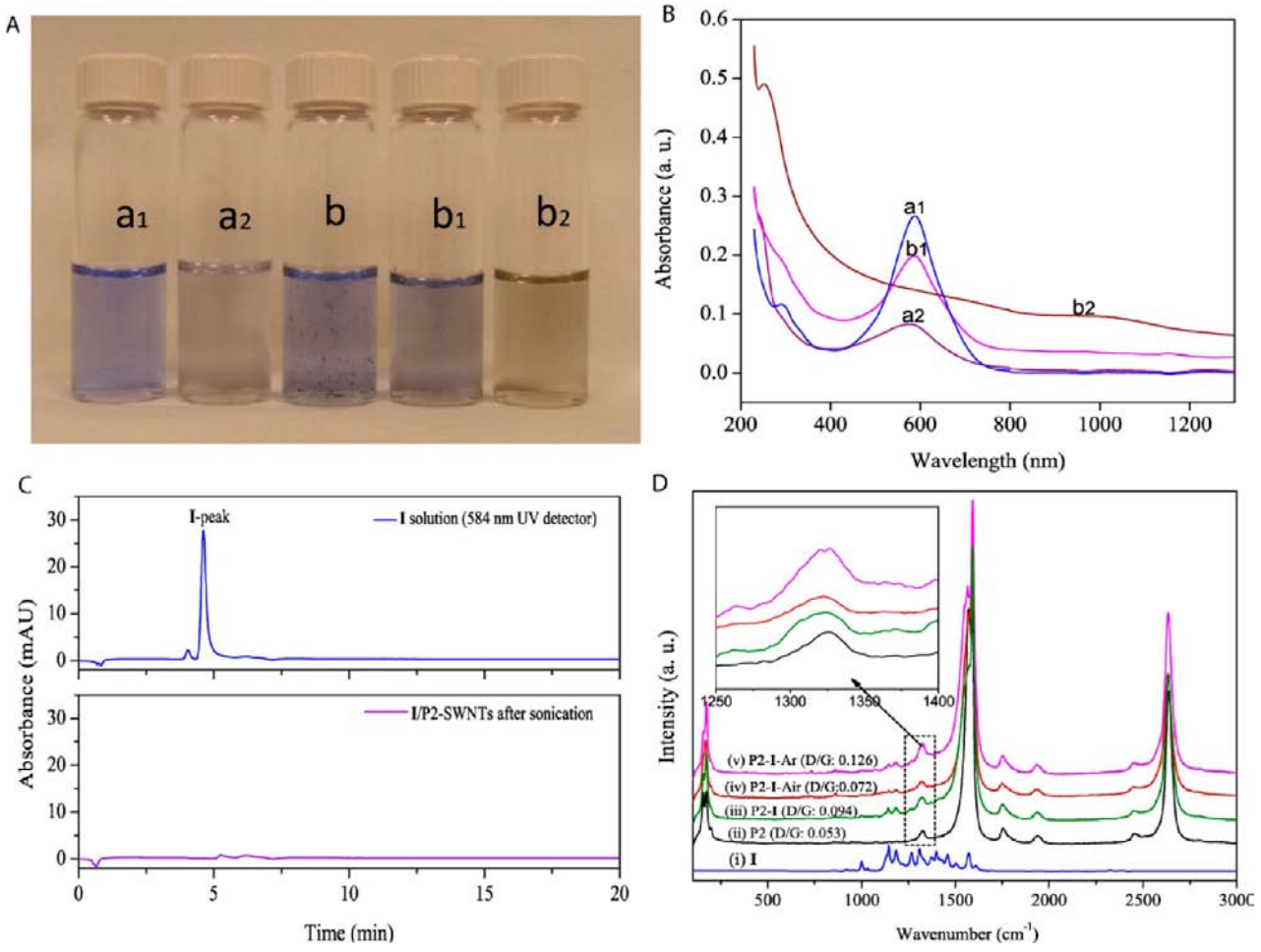

Figure 6. Treatment of P2 SWNT samples with **I** using different conditions. (A) Photographic images and (B) UV−vis−NIR spectra of (a) **I**/water solution (a1) before and (a2) after ultrasonication for 1 h in an ice-bath. Photographic images of (b) **I**/P2-SWNTs mixture (b) before ultrasonication, (b1) after 15 min ultrasonication, and (b2) after 1 h ultrasonication. (C) HPLC chromatogram of 20 μL of 1 μM **I** before and after ultrasonication with P2-SWNTs. UV-detector 584 nm was used. The peak at 4.60 min in HPLC spectrum is identified as the **I** peak. Column: Agilent Eclipse Plus C18, 3.5 μM, 4.6 × 100 mm. Elute condition: 50% acetonitrile (ACN):water, 0.15 mL/min. (D) Raman spectra of (i) powder **I**, (ii) Pristine P2-SWNTs, (iii) Ppt of (P2-SWNTs-**I**), (iv) Ppt of (P2-SWNTs-**I**-Air), and (v) Ppt of (P2-SWNTs-**I**-Ar). Inset of D is the enlarged view of D-band evolution of Ppt-SWNTs under various conditions.

limited quantities of radicals which are also selective to metallic nanotubes.[59−61] In our separation method, we treat P2-SWNT with **I** at 60 °C followed by ultrasonication. Heating likely causes the fairly large **I** molecule to wrap around the nanotubes to suspend; the nanotubes "clumps" visibly "dissolve" when the solution is heated. Ultrasonication helps to generate radicals which will meet and react with the nanotubes during the heating cum stirring step. We postulate that the generated radicals, particularly if present in limited amounts, have selective preference for metallic nanotubes over semiconducting nanotubes due to the higher electron density of states at their Fermi levels and smaller ionization potential.[39,62] Since aromatic azo compounds with resonance stabilization degrade little even under sonication, these compounds produce suitable amounts of radicals for selective attack on metallic nanotubes.

To confirm our hypothesis of radical formation with **I**, we investigated the degradation of **I** molecules (decolourization), with and without nanotubes, under ultrasonication in water (Figure 6A, B, and Supplementary Experimental Section B for details). Degradation was monitored by UV−vis spectroscopic and high-performance liquid chromatography (HPLC) analysis. **I** molecules are degraded in water after ultrasonication for 1 h; after ultrasonication for 1 h (Figure 6A, a2), there was visual color change compared to that before ultrasonication (Figure 6A, a1). The UV−vis spectra of control **I** solution before and after ultrasonication process (Figure 6B (a_1, a_2)) shows that the azo peak (at around 587 nm) weakens with sonication, indicative of azo bond degradation. With **I** in the presence of P2-SWNTs, we observed more blue color decrease visually (Figure 6A (b, b1, b2) and complete disappearance of the **I** UV−vis−NIR peak (Figure 6B, (b1, b2), i.e. degradation of **I**, in the presence of P2-SWNTs after 1 h of ultrasonication. Further, the degradation of **I** was studied by HPLC. **I** was chromatographed by injecting 20 μL of 1 μM **I** solution, then detecting the corresponding peak at its maximum wavelength, in order to determine the retention time of **I**. Using UV detector (584 nm), a strong single peak of **I** was observed at 4.60 min (Figure 6C). Under the same HPLC condition, ultrasonicated **I**/P2-SWNTs sample does not give any peak of **I** at 4.60 min confirming the complete decolurizaiton/degradation of **I** after ultraonication (Figure 6C). These experiments prove that the ultrasonication step significantly degrades **I** molecules, particularly the azo bond, to generate degradation products.[62]

dx.doi.org/10.1021/ja312282g | J. Am. Chem. Soc. 2013, 135, 5569−5581

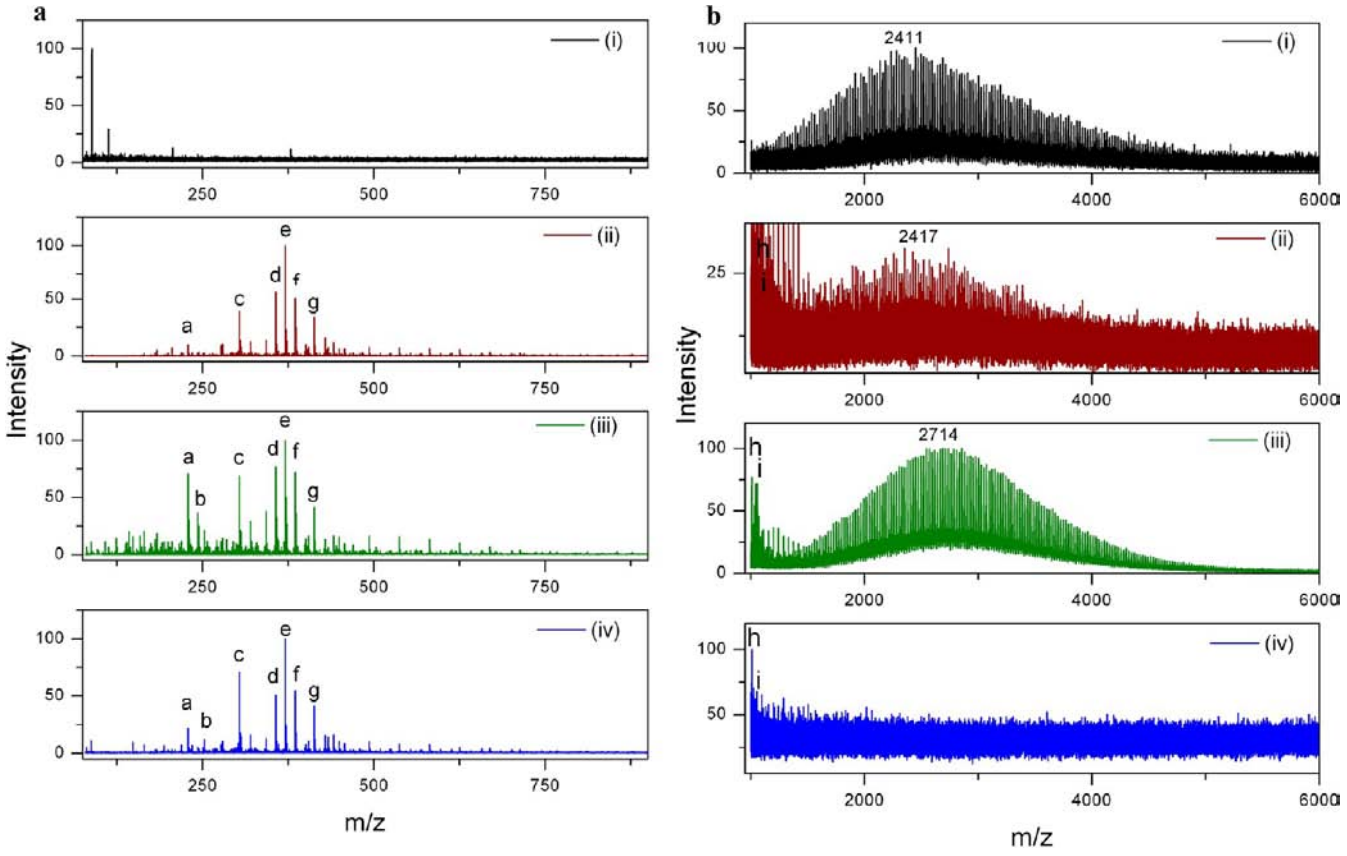

Figure 7. Normalized mass spectra of (i) pristine P2-SWNTs (control), (ii) Supt SWNTs, (iii) Ppt-SWNTs, and (iv) **I**. (a) Low m/z fragments. (b) High m/z fragments (starting with P2 samples).

To further confirm our hypothesis that radicals are generated by ultrasonication and react with the nanotubes, P2-SWNTs were ultrasonicated separately with **I** under various conditions (Figure 6D): (ii) in water with "normal" dissolved oxygen as in separation experiments for Figure 2; (iii) in water aerated with Air (the dissolved O_2 which is a radical quencher is increased[63]) and (iv) in water aerated with Argon gas (inert Ar gas aeration can purge the dissolved oxygen and results in less radical quenching[64]) (see Supplementary Experimental Section C). The main objective of this study is to control the radicals produced during the ultrasonication with P2-SWNTs. We found that the D band that results after the different ultrasonications are dependent on the dissolved oxygen content. As shown in Figure 6D, the ratio of D-band to G band (D/G) for (ii) Pristine P2-SWNTs, (iii) Ppt of P2-SWNTs-**I**, (iv) Ppt of P2-SWNTs-**I**-Air, and (v) Ppt of P2-SWNTs-**I**-Ar were found to be 0.053, 0.094, 0.072, and 0.126, respectively. For the Ppt-SWNTs under (oxygen) Air atmosphere (iv), compared to the pristine P2 sample (ii), there is only a small though measurable change in the D band of (D/G ratio = 0.072), but there is a large increase in the D band of Ppt-SWNTs-argon sample (0.126). The argon aeration removes the dissolved oxygen so that more radicals are present during the ultrasonication process in (v). These results substantially prove that degradation products of **I** produced under ultrasonication are radicals which can be quenched by oxygen. In contrast, under Argon gas environment, more radicals are produced that can attack SWNTs in higher reaction rates which is confirmed by the large D band of Ppt-SWNTs-Ar (Figure 6D, curve v).

We also demonstrate the m-SWNTs selectivity of **I**/DP-**I** with P2-SWNTs below. Selective reaction of **I**/DP-**I** with m-SWNTs is corroborated by the Raman spectra of Ppt-SWNTs after complete removal of unreacted or physically adsorbed **I**/DP-**I** using DMF solvent (Figure 2b and c). A small disorder peak (D-band) at 1324 cm^{-1} due to the defects of nanotubes was observed for the pristine-P2-SWNTs sample (Figure 2c, curve i). The Raman spectrum of Ppt-SWNTs fraction showed an increased D-band as compared with Supt-SWNTs (Figure 2c, curves iii and ii). The D-band is a measure of covalent reaction on the nanotubes. The Raman D-band increase only in the Ppt-SWNTs, together with the UV−vis−NIR data (Figure 2a), supports our hypothesis that metallic nanotubes selectively reacted and were cross-linked with the naphthyl radicals and become denser compared to the semiconducting nanotubes so that the reacted species can be separated by using normal centrifugation and DGU. The dye **I** which contains multiple azo bonds likely evolve diradicals leading to cross-linking and bundling of the nanotubes. The AFM image of Ppt-SWNTs (Supplementary Figure S7) shows bundles of nanotubes in Ppt-SWNTs fraction (The Ppt-SWNTs were highly agglomerated after normal centrifugation. For the AFM measurements, we redispersed the Ppt-SWNTs in a cosurfactant solution (1% SDS/SC)).

Matrix-assisted laser desorption/ionization coupled with time-of-flight mass spectrometry (MALDI-TOF-MS) was used to help confirm the preferential reaction of decomposed **I** fragments with m-SWNTs. Figure 7 (and also Supplementary Figure S8 and Table S4) shows the mass to charge (m/z) spectra of (i) pristine-SWNTs, (ii) separated Supt s-SWNTs,

dx.doi.org/10.1021/ja312282g | J. Am. Chem. Soc. 2013, 135, 5569−5581

(iii) separated Ppt m-SWNTs, and (iv) pure **I**. The separated SWNTs were washed several times with distilled water before the MALDI-TOF-MS runs. The left panel (Figure 7a) shows the low m/z values corresponding to **I** fragments, while the right panel (Figure 7b) shows the mass distribution of the carbon nanotube fragments. The comparison of the low m/z spectrum of compound **I** with that of pristine SWNTs (Figure 7a(iv), (i)) shows several peaks due to degraded fragments of **I**. Supplementary Table S4 shows the proposed structures of major degradation products (**a**−**i**) of **I**, identified based on the MALDI-MS studies. Fragmentation peaks of **I** (**a**−**i**, Figure 7a(iv)) were also observed in the mass spectra of Supt-SWNTs and Ppt-SWNTs (Figure 7a(ii) and a(iii), respectively). It appears that the intensities of the two smaller fragments (**a**−**b**), which each contain a single naphthyl ring, are significantly suppressed in Supt-SWNTs (ii) compared with Ppt-SWNTs (iii) while the larger fragments (particularly, **c**−**g**) which contain two naphthyl rings each, have approximately the same relative intensity distribution in Supt-SWNTs, Ppt-SWNTs, and **I**. We infer that **I** decomposes to naphthyl radical which has sufficient reactivity to preferentially attack m-SWNTs over s-SWNTs. This is further corroborated by the high m/z mass spectra of the various nanotube fractions in Figure 7b, elaborated below.

P2-SWNTs when ionized produce carbon clusters (C_n) of varying sizes (Figure 7b(i)). Singly charged carbon clusters, C^+_n, with m/z peak centered at ∼2411 (n = ∼200), (n = ∼94−350) were observed for pristine P2-SWNTs.[65,66] For the Supt s-SWNTs (Figure 7b(ii)), a mass distribution of carbon clusters with a shape similar to that of pristine P2-SWNTs was observed with m/z maximum centered at ∼2417. In contrast, for Ppt m-SWNTs (Figure 7b(iii)), the maximum of the ionized carbon clusters population intensity is shifted by m/z of 297 toward a significantly higher m/z value, with a maximum at ∼2714. This is possibly due to the attachment of degradation products of **I** to metallic nanotubes. Supplementary Table S4 lists the possible degradation products that could be attached to Ppt m-SWNTs, and the main degradation products with m/z of around 297 are identified to be naphthyl-based compounds with amine and sulfonic groups. The significant shift in the carbon clusters maximum peak position to ∼2714 (m/z) (Figure 7b(iii)), together with the observed increased **a** and **b** peak intensities in the lower m/z fragment range (Figure 7a(iii)) in Ppt-SWNTs but not in Supt-SWNTs, corroborates our hypothesis that degradation of **I** to smaller fragments (DP-**I**, degradation products of **I**) occurs during the sonication/standing process, and that these fragments preferentially react with m-SWNTs.

Large area X-ray photoelectron spectroscopy (XPS) was used to measure the surface composition of the separated Supt s-SWNTs and Ppt-SWNTs fractions after standing with **I** (followed by washing with distilled water). Table 1 shows the estimated atomic concentrations of carbon, oxygen, nitrogen, and sulfur in the pristine nanotubes, separated tubes, and control **I** (Supplementary Figure S9).[67] Separated s-SWNTs and Ppt-SWNTs showed two peaks, not present in pristine nanotubes, centered at 164.0 and 398.4 eV which were assigned to S2p and N1s, respectively (Supplementary Figure S9); these arise from **I**/DP-**I**. The theoretical C, N, O, and S contents of **I** are 46.65, 9.52, 20.20, and 12.45%. The higher N1s, O1s, and S2p contents in Ppt-SWNTs compared with Supt-SWNTs corroborate the hypothesis that the former fraction has more of the DP-**I**/**I** that cannot be washed away easily because of selective covalent reaction. We also investigated the zeta potential (ζ) of the Supt-SWNTs and Ppt-SWNTs fractions after separation with anionic **I** molecules (Table 2). The more negative ζ (49.40 ± 1.03 mV) of Ppt-SWNTs compared to Supt-SWNTs and control **I** solution further corroborates that the DPs of **I** which contains more sulfonic groups reacted and cross-linked the nanotubes to sink them into Ppt-SWNTs (Table 2).

We performed density functional calculations to model the interaction of 2-naphthyl radical with various semiconducting (specifically (14, 4), (12,8), (14,7), (19,0) and metallic (15,3), (18,0), (12,9), (15,6)) SWNTs. The binding energies of 2-naphthyl radical are similar (scatter of order 0.1−0.2 eV in these samples) for each type of SWNTs (semiconducting/metallic). We found that the 2-naphthyl radical binds with the semiconducting and metallic SWNTs studied with binding energy ranges of about (∼ −0.70 to −0.80 eV) and (∼ −0.90 to −1.10 eV), respectively, with the formation of a C−C bond of about ∼1.57 Å length (Figure 1c). The calculated binding energies of 2-naphthyl radical to various nanotube species are listed in Table 3. The higher binding energies, by about 0.20−0.30 eV, of 2-naphthyl radical to metallic SWNTs, i.e. (15,3), (18,0), (12,9), and (15,6), indicate that the 2-naphthyl radical

Table 1. Atomic Concentrations of Oxygen, Nitrogen, Carbon, and Sulfur in (i) P2-SWNTs, (ii) Supt-SWNTs, (iii) Ppt-SWNTs, and (iv) I

sample	C1s position (eV)	C1s (%)	O1s (%) (531.8 eV)	N1s (%) (398.4 eV)	S2p (%) (164.0 eV)
(i) pristine-P2-SWNT	284.6	97.68	2.32		
(ii) Supt-SWNTs	283.8	90.75	7.57	0.99	0.69 (1.32)[a]
(iii) Ppt-SWNTs	284.1	87.08	10.3	2.03	0.75 (2.71)[a]
(iv) **I**		46.65	20.20	9.52	12.45

[a]Calculated S value based on the N value and the ratio of undecomposed **I**.

Table 2. Zeta Potential (ζ) Value of I, Supt-SWNTs, and Ppt-SWNTs in Water (pH 7.0) Starting with P2 Samples

sample no.	samples	mobility	zeta potential (mV)
1	DB71 (**I**)	−2.92	−37.35 ± 2.60
2	Supt-s-SWNTs	−0.79	−10.07 ± 1.67
3	Ppt-m-SWNTs	−3.86	−49.40 ± 1.03

Table 3. Binding Energies of 2-Naphthyl Radical with s- and m-SWNTs

	type	diameter (Å)	binding energy (eV) 2-naphthyl radical
SWNT (14,4)	sc	12.89	−0.73
SWNT (12,8)	sc	13.73	−0.78
SWNT (14,7)	sc	14.55	−0.73
SWNT (19,0)	sc	14.87	−0.79
SWNT (15,3)	m	13.14	−1.06
SWNT (18,0)	m	14.11	−1.07
SWNT (12,9)	m	14.33	−0.99
SWNT (15,6)	m	14.72	−0.89

dx.doi.org/10.1021/ja312282g | J. Am. Chem. Soc. 2013, 135, 5569−5581

prefers to bind to the metallic SWNTs rather than to the semiconducting SWNTs studied. There is no discernible trend of binding energy with diameter for the s-SWNTs but a suggestion of a trend of weaker binding with larger diameter m-SWNTs. There is also a suggestion that the binding energies to m- and s-tubes may converge to similar values at larger diameter.

To confirm the differential reactivity of **I**/DP-**I** with pure metallic versus semiconducting SWNT, we used sorted ultrapure metallic and semi-SWNTs (supplied from Nano-Integris), instead of unsorted P2-SWNTs. (We note the pristine NanoIntegris ultrapure metallic SWNTs have higher D band than the pristine NanoIntegris ultrapure semiconducting SWNTs.) The ultrapure metallic and semi-SWNTs were also treated with **I** in water by ultrasonication. As shown in Figure 5c, a relatively higher increase in the D band after ultrasonication was observed for metallic tubes than semiconducting ones, confirming preferential reactivity of the radicals with metallic nanotubes. The larger D band increase is despite the fact that the ultrapure metallic nanotubes are less well-suspended than the ultrapure semiconducting nanotubes and thus have less sidewall exposed due to bundling (Figure 5a).

Various techniques described above confirm the preferential reaction of **I**-DP with m-SWNTs and solvation of s-SWNTs by undecomposed **I**. The selection mechanism of our **I** is summarized in Figure 1d. The pristine **I** preferentially suspends the s-SWNTs, and the m-SWNTs are poorly suspended by **I**. Further, **I** decomposes into limited amounts of radicals (and also diradicals) that preferentially attack the m-SWNTs which tend to remain bundled and settle down to the bottom. Our undecomposed azo dye is itself a dispersant which is also selective, but to the other species (semiconducting), so that it preferentially suspends s-SWNTs while its decomposition products selectively react with m-SWNTs, resulting in the settling, under centrifugation, of a higher proportion of the m-SWNTs than of the s-SWNTs. It appears that the presence of highly solvating and electron-withdrawing sulfonate groups makes **I** a s-SWNT selective agent as well as a good dispersant. The stability of **I** permits it to selectively disperse/suspend s-SWNTs during the long-standing period.

We show for the first time that sulfonate functionalized naphthalene azo dye is highly metallicity-based selective. We propose that the separated Ppt m-SWNTs are preferentially reacted with DPs of **I** via a radical reaction. Aromatic azo compounds have hitherto not been used in the separation of nanotubes, but we find that this class of compounds offers the subtlety in the control of radical concentration and reactivity needed to achieve high efficiency metallicity-based selection. Aromatic azo compounds are known to be rather stable and have been used as dyes although long-term standing, heat, sonication, and so forth can slowly decompose them to radicals at relatively low concentration.[60,61,68] Further, the resonance stabilization afforded by the naphthalene ring results in greater stability of the original compound **I** and the naphthyl radical compared to previously reported compounds.[25,35−37,39] The stabilities of various aromatic azo compounds measured by their reduction potentials are summarized in Supplementary Table S5, and it can be seen that our compound **I** is relatively stable (with more negative reduction potential). For the radicals generated to be selective only for m-SWNTs, they must be rather less aggressive and more stable but nonetheless reactive and must be present at low or limiting concentrations. The subtly reactive naphthyl radical produced in controllably low concentration by decomposition of **I** appears to be selectively reactive to m-SWNTs.

Our report here is the first report of high performance transistor behavior achieved with simple high yield/high purity selective chemistry-based separation. Liu et al. have reported outstanding purity and yields of single chirality and metallicity-based separation with gel chromatography-assisted method.[69] However, there is no report on transistor performance with their gel-separated nanotubes. The yields and purities of their various separated fractions vary vastly while our calculation here is based on the all chiralities present in the sample here. Kim et al. reported metallicity-based sorting of SWNTs by free solution electrophoresis and density gradient centrifugation techniques for HiPco and laser ablated nanotubes.[70] They achieved outstanding on/off ratios for some of the sorted nanotubes, and the achieved separation purities are about 76−78%, instead of the 93% achievable here. The OFF current of our semiconducting nanotube device ($\sim 10^{-10}$) is relatively 1 order of magnitude higher than that of reported single nanotube semiconducting devices.[70] This may due to the presence of multiple nanotubes in the electrode channel that can decrease channel resistance of devices compared to single nanotube devices.[70] But, our few nanotube device's OFF current is almost similar with the OFF current ($\sim 10^{-10}$) of single semi-SWNT devices prepared by ac-dielectrophoresis method.[71] Our transfer characteristic (Figure 3c) shows hysteresis which may be due to impurities such as surfactant. These impurities can act as charge trapping center on the surface of SWNTs and need to be removed in future work.[72,73]

Our current finding points to a totally new family of selective chemicals based functionalized polycyclic aromatic-based azo dyes. **I** is dual-selective. The relatively stable radicals produced appear to preferentially attack m-SWNTs, and the functionalized polycyclic aromatic group selectively suspends/solubilizes s-SWNTs. This method is simple and can be easily employed for large scale production of high purity s-SWNT for commercial and industrial applications. In contrast to DGU assisted separation, which requires high speed centrifugation and results in very low semiconducting nanotubes yield of about 1.0%, our method uses normal centrifugation method to result in high purity (with $S_{22} \sim 93\%$) and significantly higher yield (up to 41%). Our separation method can process large volumes of nanotubes simultaneously as the process mainly involves standing the sample in beakers and then centrifuging the treated samples. DGU is more volume-limited due to the mechanical limits of the ultra high speed centrifugation apparatus. Hence, the main advantage of our method is high yield and high volume compared to DGU assisted separation. In addition, our new method is more cost-effective than DGU method as the latter requires highly sophisticated equipment with expensive rotors. Another important advantage of this work is that **I** also functions as a surfactant to disperse selectively s-SWNT, so we can avoid cosurfactants usually required for the preparation of good SWNT dispersions.

■ CONCLUSIONS

In summary, we have successfully enriched semiconducting SWNT fractions from arc-discharge P2-SWNTs using **I**, the first reported example of a new class of separation/dispersant agent based on an azo compound. Raman and UV−vis−NIR results confirm that metallic SWNTs are depleted from the semiconducting enriched Supt-SWNTs samples. Highly pure,

>93% semiconducting, nanotubes with high yield (up to 41%) can be obtained via our proposed method using centrifugation. XPS, Raman, and UV−vis−NIR results indicate preferential molecular charge transfer between undecomposed **I** and s-SWNTs. The radical formation with ultrasonication of **I** was proved by visual color change observations and UV−vis−NIR. Based on the D-band of Raman spectroscopy, MALDI-TOF-MS, and density functional calculations analysis, we find that degradation products of **I** preferentially react with metallic-SWNTs. **I** is a naphthalene azo dispersing agent that adsorbs preferentially on semiconducting nanotubes but decomposes slowly to form fairly stable radicals that preferentially react with metallic nanotubes, so that the DP-**I**/m-SWNT hybrids settle under centrifugation. Semiconducting SWNTs are selectively suspended and separated from m-SWNTs. We have also demonstrated p-type pure semiconducting FET devices with a good ON/OFF ratio and excellent field effect mobility. This is a very simple method for the separation and purification of semiconducting SWNTs with high yield. With density gradient ultracentrifugation, >98% semiconducting SWNTs can be obtained with a single pass of purification. We believe that this inexpensive novel selective chemical separation method can be easily employed for large scale production of semiconducting nanotubes for electrical and electronic applications.

METHODS

Chemicals and Reagents. P2-SWNTs were purchased from Carbon Solutions, Inc. (CA, USA). Direct blue 71 (**I**), sodium dodecyl sulfate (SDS), and sodium cholate (SC) were from Sigma-Aldrich, USA. All other chemicals were ultrapure analytical grade reagents and were used without further purification.

Separation of SWNTs. Solution processing of Pristine P2-SWNTs was carried out in the following manner. A solution of 15 mg arc-discharge P2-SWNTs in 1×10^{-3} M solution of **I** in water was stirred and heated at 60 °C for 45 min and then ultrasonicated using a 130-W Ultrasonic Processor equipped with a 6 mm flat tip probe (VCX130, Sonics & Materials, Inc., USA) for 1 h at a power intensity of 32 W/cm^2. After ultrasonication, the resulting solution was kept standing for two days at room temperature (Step (i), Figure 1b). In Step (ii), P2-SWNT/**I** solution was transferred into centrifuge tubes and then centrifuged at 50 000 (to 100 000) g with a fixed angle rotor for 1 h. Then, the supernatant SWNT (Supt-SWNT) solution was quickly decanted from the tube without disturbing the precipitate. The separated Supt-SWNT solution was washed with doubly distilled water through a polycarbonate membrane (pore size 0.2 μm), to remove excess or unreacted **I** molecules from the SWNTs, and the solids on the filter were then washed repeatedly several times with distilled water (Step (ii), Figure 1b). Finally, the separated Supt-SWNTs were redispersed in 1% sodium dodecyl sulfate (SDS) and sodium cholate (SC) cosurfactant solution (1:4 SDS/SC) with an ultrasonic probe for 30 min (Step (iii), Figure 1b). Precipitated-SWNTs (Ppt-SWNTs) (collected from Step (ii), Figure 1b) were redispersed in 1% surfactant solution (1:4 SDS/SC) after repeated washing with doubly distilled water. The buoyant densities of Supt-SWNT (1.064 g/cm^3) and Ppt-SWNT (1.189 g/cm^3) were estimated using a density gradient column.[14,54]

Density Gradient Ultracentrifugation (DGU). A density gradient column was formed in a 13 mL centrifuge tube by layering with increasing concentrations of iodixanol (Optiprep, Sigma-Aldrich). The bottom layer was filled with 50% w/v iodixanol, followed by 36%, 20%, and 12% w/v iodixanol as the top layer of the density gradient. Each layer contained 1% w/v sodium cholate (SC, 99%, Sigma-Aldrich). The P2-SWNT/**I** solution to be ultracentrifuged was prepared as described above (*Separation of SWNTs*) up to the point of centrifugation. After two days standing, the P2-SWNT/**I** solution (containing both s-SWNTs and m-SWNTs) was filtered/washed with distilled water through a 0.2 μm pore polycarbonate membrane, and the solids were redispersed in 1% SC solution. For the control experiment, Pristine P2-SWNTs (without **I**) were dispersed in 1% SC. The P2-SWNT/**I**/SC or P2-SWNT/SC solution was inserted on top of the density gradient column with a syringe. Density gradient ultracentrifugation was performed at RCF (relative centrifugal force) max 200 000*g* for 6 h using a Hitachi CP100WX P40ST swing-bucket rotor. After ultracentrifugation, the layers of the stratified column were successively extracted with a micropipet.

Characterization of SWNTs. Pristine-P2-SWNTs were used as the control in all of the characterization experiments. Pristine P2-SWNTs (control) and the **I**-treated Supt-SWNTs and Ppt-SWNTs fractions were prepared similarly, unless otherwise stated, for all of the characterization experiments. UV−vis−NIR absorption spectra were measured using a Varian Cary 5000 UV−vis−NIR spectrophotometer. Before characterization of pristine-SWNTs and separated SWNTs, all nanotube fractions were thoroughly washed with distilled water and then with dimethylformamide (DMF) (by stirring and filtration) to remove **I** and organic impurities. The purity of the separated semiconducting Supt *s*- SWNT sample was estimated through calculation of the ratio $A_S/(A_M + A_S)$,[70,74,75] where A_S and A_M are respectively the areas of the S_{22} and M_{11} absorption peaks determined by curve fitting analysis[70,74,75] (see Supplementary Figures S2 and S3). Raman spectra were measured with a Renishaw Raman scope in backscattering configuration using 633 nm wavelength laser over SWNT solid samples. Laser power of 2.5−5.0 mW was used to prevent destruction of the SWNT samples during measurement. For Raman measurements, after extensive washing, the Supt-SWNTs and Ppt-SWNTs samples were redispersed in a cosurfactant (1:4 SDS:SC) solution.

A MALDI-TOF/TOF-MS (Model 4800, AB SCIEX, Toronto, Canada) was used to measure the molecular weight (MW) of the molecules. The laser power was set to 3500 units. Mass spectra (MS) were acquired in positive reflector mode with 900 laser shots. Atomic force microscopy (AFM) was conducted using a MFP 3D microscope (Asylum Research, Santa Barbara, CA) with a cantilever (Arrow NC, Nanoworld) in ac mode. The scan rate was set to 1 Hz at various scan sizes. X-ray photoelectron spectroscopy (XPS) measurements were made using a Kratos Axis-ULTRA X-ray photoelectron spectroscope with a monochromatic Al-Kα X-ray source (1486.7 eV) in an ultrahigh-vacuum environment of 10^{-9} Torr. Survey spectra were made with a pass energy of 160 eV and a step size of 1 eV, and high-resolution spectra were made with a pass energy of 40 eV and a step size of 0.1 eV. Electrical properties measurements on field effect transistors (FETs) made with separated s-SWNTs were carried out in ambient environment using a Keithley semiconductor parameter analyzer, model 4200-SCS. High-performance liquid chromatography (HPLC) analysis was carried out with an Agilent 1100 series. The separation was tested on an Agilent Eclipse Plus C18 column (100 × 4.6 mm i.d., 3.5 μm). The mobile phase was water/acetonitrile (50:50, v/v) in isocratic eluent at a constant flow rate of 0.15 mL/min. The injection volume was 20 μL. UV−vis detection was run at 584 nm wavelength.

Field Effect Transistor Fabrication. Field effect transistors were fabricated by alignment of purified s-SWNTs in the channel regions of prepatterned electrodes using an applied AC electric field. A frequency generator was used to apply 3 V (peak-to-peak) at 2 MHz across the source and drain electrodes. Ten μL of the s-SWNT suspension was placed on each channel gap of the electrode-patterned substrate using a pipet and was aligned for 10 s under the ac electric field. After 10 s, the SWNT suspension was gently blown off, and the sample was characterized with AFM. Back-gated SWNT-FETs were fabricated on a heavily doped p-type silicon wafer capped with a 300 nm thick thermally grown silicon dioxide (SiO_2) layer. Heavily doped p-type silicon was used as the back-gate. The source and drain electrodes were deposited as 5 nm/50 nm of Ti/Au with channel length (L) of 2−3 μm. To estimate the effective hole mobility (μ_{eff}) of s-SWNT FET devices, the following equation was adopted:[76]

dx.doi.org/10.1021/ja312282g | J. Am. Chem. Soc. 2013, 135, 5569−5581

$$\mu_{\text{eff}} = \frac{L}{C/L} \cdot \frac{1}{V_d} \cdot \frac{dI_d}{dV_g} \quad (1)$$

where L is the channel length, I_d is the drain current, V_g is the gate voltage, $C/L = 2\pi\varepsilon\varepsilon_{ox}/\ln(2h/r)$ is the gate capacitance per unit length,[76] r and h are radius of the SWNTs and the equivalent oxide thickness of SiO_2 (dielectric) (300 nm), ε_{ox} is the permittivity of the SiO_2 (3.9), and ε is the permittivity of free space.

Density Functional Calculations. The bonding with SWNT sidewall of radicals resulting from the decomposition of **I** was numerically simulated. All of the calculations in the computer simulations were performed using generalized gradient approximation Perdew–Burke–Eznerhof (GGA-PBE) method[77] as implemented in the Vienna Ab initio Simulation Package (VASP).[78−80] A 1 × 1 × 1 grid for k-point sampling and an energy cutoff of 400 eV were used throughout the calculations. All atomic coordinates were optimized until the forces acting on each atom were less than 0.01 eV/Å. The 2-naphthyl radical was used as the model radical from decomposed **I** to understand the interaction between **I** and its DPs with SWNTs. Semiconducting SWNT species (14,4), (12,8), (14,7), and (19,0) and metallic species (15,3), (18,0), (12,9), and (15,6) all with diameters of about 14 Å, were selected as representative of the species distribution of arc-discharge P2-SWNTs.

■ ASSOCIATED CONTENT

Ⓢ Supporting Information

Experimental details of SWNTs treatment with **I** under an air and argon environment, images of DGU separated nanotubes, purity and yield calculations, density profile of density gradient medium, AC-dielectrophoresis, Raman spectra, AFM image, mass spectra, and photoelectron spectra of separated nanotubes. s-SWNTs yield calculation, table of Raman vibrational bands of **I**, atomic concentrations of the various fractions, list of degradation products from MALDI-MS-TOF spectra analysis, and reduction potentials of azo compounds. This material is available free of charge via the Internet at http://pubs.acs.org.

■ AUTHOR INFORMATION

Corresponding Author

mbechan@ntu.edu.sg; KokHwa@ntu.edu.sg

Author Contributions

A.K.S. and S.M. contributed equally to this manuscript.

Notes

The authors declare no competing financial interest.

■ ACKNOWLEDGMENTS

This work was supported by a Competitive Research Program grant from the Singapore National Research Foundation (NRF-CRP2-2007-02).

■ REFERENCES

(1) Avouris, P.; Chen, Z.; Perebeinos, V. *Nat. Nanotechnol.* **2007**, *2*, 605.

(2) Chen, P. C.; Fu, Y.; Aminirad, R.; Wang, C.; Zhang, J. L.; Wang, K.; Galatsis, K.; Zhou, C. W. *Nano Lett.* **2011**, *11*, 5301.

(3) Nobusa, Y.; Yomogida, Y.; Matsuzaki, S.; Yanagi, K.; Kataura, H.; Takenobu, T. *Appl. Phys. Lett.* **2011**, *99*, 183106.

(4) Rouhi, N.; Jain, D.; Burke, P. J. *ACS Nano* **2011**, *5*, 8471.

(5) Reich, S.; Thomsen, C.; Maultzsch, J. *Carbon Nanotubes: Basic Concepts and Physical Properties*; Wiley: New York, 2004.

(6) Bradley, K.; Gabriel, J. C. P.; Gruner, G. *Nano Lett.* **2003**, *3*, 1353.

(7) Hersam, M. C. *Nat. Nanotechnol.* **2008**, *3*, 387.

(8) Lee, H. W.; Yoon, Y.; Park, S.; Oh, J. H.; Hong, S.; Liyanage, L. S.; Wang, H. L.; Morishita, S.; Patil, N.; Park, Y. J.; Park, J. J.; Spakowitz, A.; Galli, G.; Gygi, F.; Wong, P. H. S.; Tok, J. B. H.; Kim, J. M.; Bao, Z. A. *Nat. Commun.* **2011**, *2*, 541.

(9) Liu, J.; Hersam, M. C. *MRS Bull.* **2010**, *35*, 315.

(10) Snow, E. S.; Campbell, P. M.; Ancona, M. G.; Novak, J. P. *Appl. Phys. Lett.* **2005**, *86*, 033105.

(11) Zhou, Y. X.; Gaur, A.; Hur, S.; Kocabas, C.; Meitl, M. A.; Shim, M.; Rogers, J. A. *Nano Lett.* **2004**, *4*, 2031.

(12) Maeda, Y.; Kimura, S.-i.; Kanda, M.; Hirashima, Y.; Hasegawa, T.; Wakahara, T.; Lian, Y.; Nakahodo, T.; Tsuchiya, T.; Akasaka, T.; Lu, J.; Zhang, X.; Yu, Y.; Nagase, S.; Kazaoui, S.; Minami, N.; Shimizu, T.; Tokumoto, H.; Saito, R. *J. Am. Chem. Soc.* **2005**, *127*, 10287.

(13) Anilkumar, P.; Fernando, K. A. S.; Cao, L.; Lu, F. S.; Yang, F. C.; Song, W. L.; Sahu, S.; Qian, H. J.; Thorne, T. J.; Anderson, A.; Sun, Y. P. *J. Phys. Chem. C* **2011**, *115*, 11010.

(14) Arnold, M. S.; Green, A. A.; Hulvat, J. F.; Stupp, S. I.; Hersam, M. C. *Nat. Nanotechnol.* **2006**, *1*, 60.

(15) Bachilo, S. M.; Balzano, L.; Herrera, J. E.; Pompeo, F.; Resasco, D. E.; Weisman, R. B. *J. Am. Chem. Soc.* **2003**, *125*, 11186.

(16) Berton, N.; Lemasson, F.; Tittmann, J.; Sturzl, N.; Hennrich, F.; Kappes, M. M.; Mayor, M. *Chem. Mater.* **2011**, *23*, 2237.

(17) Chen, Z.; Du, X.; Du, M.-H.; Rancken, C. D.; Cheng, H.-P.; Rinzler, A. G. *Nano Lett.* **2003**, *3*, 1245.

(18) Collins, P. C.; Arnold, M. S.; Avouris, P. *Science* **2001**, *292*, 706.

(19) Debnath, S.; Cheng, Q. H.; Hedderman, T. G.; Byrne, H. J. *Carbon* **2010**, *48*, 1489.

(20) Krupke, R.; Hennrich, F.; Lohneysen, H.; Kappes, M. M. *Science* **2003**, *301*, 344.

(21) Schmidt, G.; Filoramo, A.; Derycke, V.; Bourgoin, J. P.; Chenevier, P. *Chem.—Eur. J.* **2011**, *17*, 1415.

(22) Schmidt, G.; Gallon, S.; Esnouf, S.; Bourgoin, J. P.; Chenevier, P. *Chem.—Eur. J.* **2009**, *15*, 2101.

(23) Tanaka, T.; Jin, H. H.; Miyata, Y.; Kataura, H. *Appl. Phys. Express* **2008**, *1*, 114001.

(24) Tanaka, T.; Liu, H. P.; Fujii, S.; Kataura, H. *Phys. Status Solidi: Rapid Res. Lett.* **2011**, *5*, 301.

(25) Usrey, M. L.; Lippmann, E. S.; Strano, M. S. *J. Am. Chem. Soc.* **2005**, *127*, 16129.

(26) Wei, D.; Liu, Y.; Cao, L.; Zhang, H.; Huang, L.; Yu, G.; Kajiura, H.; Li, Y. *Adv. Funct. Mater.* **2009**, *19*, 3618.

(27) Zhang, G.; Qi, P.; Wang, X.; Lu, Y.; Li, X.; Tu, R.; Bangsaruntip, S.; Mann, D.; Zhang, L.; Dai, H. *Science* **2006**, *314*, 974.

(28) Zhang, H. L.; Liu, Y. Q.; Cao, L. C.; Wei, D. C.; Wang, Y.; Kajiura, H.; Li, Y. M.; Noda, K.; Luo, G. F.; Wang, L.; Zhou, J.; Lu, J.; Gao, Z. X. *Adv. Mater.* **2009**, *21*, 813.

(29) Fernando, K. A. S.; Lin, Y.; Wang, W.; Kumar, S.; Zhou, B.; Xie, S. Y.; Cureton, L. T.; Sun, Y. P. *J. Am. Chem. Soc.* **2004**, *126*, 10234.

(30) Voggu, R.; Rao, K. V.; George, S. J.; Rao, C. N. R. *J. Am. Chem. Soc.* **2010**, *132*, 5560.

(31) Chen, Z.; Du, X.; Du, M.-H.; Rancken, C. D.; Cheng, H.-P.; Rinzler, A. G. *Nano Lett.* **2003**, *3*, 1245.

(32) Kanungo, M.; Lu, H.; Malliaras, G. G.; Blanchet, G. B. *Science* **2009**, *323*, 234.

(33) Mesgari, S.; Poon, Y. F.; Yan, L. Y.; Chen, Y.; Loo, L. S.; Thong, Y. X.; Chan-Park, M. B. *J. Phys. Chem. C* **2012**, *116*, 10266.

(34) Lu, F. S.; Meziani, M. J.; Cao, L.; Sun, Y. P. *Langmuir* **2011**, *27*, 4339.

(35) Dai, Z.; Yan, L. Y.; Alam, S. M.; Feng, J. L.; Mariathomas, P. R. D.; Chen, Y. A.; Li, C. M.; Zhang, Q.; Li, L. J.; Lim, K. H.; Chan-Park, M. B. *J. Phys. Chem. C* **2010**, *114*, 21035.

(36) Li, J. B.; Luan, X. N.; Huang, Y. X.; Dunham, S.; Chen, P.; Rogers, J. A.; Chan-Park, M. B. *RSC Adv.* **2012**, *2*, 1275.

(37) Zhao, J. W.; Lee, C. W.; Han, X. D.; Chen, F. M.; Xu, Y. P.; Huang, Y. Z.; Chan-Park, M. B.; Chen, P.; Li, L. J. *Chem. Commun.* **2009**, 7182.

(38) Lee, C. W.; Han, X. D.; Chen, F. M.; Wei, J.; Chen, Y.; Chan-Park, M. B.; Li, L. J. *Adv. Mater.* **2010**, *22*, 1278.

(39) Strano, M. S.; Dyke, C. A.; Usrey, M. L.; Barone, P. W.; Allen, M. J.; Shan, H.; Kittrell, C.; Hauge, R. H.; Tour, J. M.; Smalley, R. E. *Science* **2003**, *301*, 1519.

(40) Zhang, L.; Tu, X. M.; Welsher, K.; Wang, X. R.; Zheng, M.; Dai, H. J. *J. Am. Chem. Soc.* **2009**, *131*, 2454.

(41) Nicholas, R. J.; Mainwood, A.; Eaves, L. *Philos. Trans. Roy. Soc. A* **2008**, *366*, 189.
(42) Itkis, M. E.; Perea, D. E.; Niyogi, S.; Rickard, S. M.; Hamon, M. A.; Zhao, B.; Haddon, R. C. *Nano Lett.* **2003**, *3*, 309.
(43) Itkis, M. E.; Niyogi, S.; Meng, M.; Hamon, M.; Hu, H.; Haddon, R. C. *Nano Lett.* **2002**, *2*, 155−159.
(44) Kim, W.-J.; Usrey, M. L.; Strano, M. S. *Chem. Mater.* **2007**, *19*, 1571.
(45) Mevellec, J.-Y.; Bergeret, C.; Cousseau, J.; Buisson, J.-P.; Ewels, C. P.; Lefrant, S. *J. Am. Chem. Soc.* **2011**, *133*, 16938.
(46) Bergeret, C.; Cousseau, J.; Fernandez, V.; Mevellec, J. Y.; Lefrant, S. *J. Phys. Chem. C* **2008**, *112*, 16411.
(47) LeMieux, M. C.; Roberts, M.; Barman, S.; Jin, Y. W.; Kim, J. M.; Bao, Z. *Science* **2008**, *321*, 101.
(48) LeMieux, M. C.; Sok, S.; Roberts, M. E.; Opatkiewicz, J. P.; Liu, D.; Barman, S. N.; Patil, N.; Mitra, S.; Bao, Z. *ACS Nano* **2009**, *3*, 4089.
(49) Anderson, N.; Hartschuh, A.; Novotny, L. *Nano Lett.* **2007**, *7*, 577.
(50) Keogh, S. M.; Hedderman, T. G.; Gregan, E.; Farrell, G.; Chambers, G.; Byrne, H. J. *J. Phys. Chem. B* **2004**, *108*, 6233.
(51) Souza, A. G.; Jorio, A.; Samsonidze, G. G.; Dresselhaus, G.; Saito, R.; Dresselhaus, M. S. *Nanotechnology* **2003**, *14*, 1130.
(52) Shin, H.-J.; Kim, S. M.; Yoon, S.-M.; Benayad, A.; Kim, K. K.; Kim, S. J.; Park, H. K.; Choi, J.-Y.; Lee, Y. H. *J. Am. Chem. Soc.* **2008**, *130*, 2062.
(53) Bergeret, C. l.; Cousseau, J.; Fernandez, V.; Mevellec, J.-Y.; Lefrant, S. *J. Phys. Chem. C* **2008**, *112*, 16411.
(54) Zhao, P.; Einarsson, E.; Lagoudas, G.; Shiomi, J.; Chiashi, S.; Maruyama, S. *Nano Res.* **2011**, *4*, 623.
(55) Banerjee, S.; White, B. E.; Huang, L.; Rego, B. J.; O'Brien, S.; Herman, I. P. *J. Vac. Sci. Technol. B* **2006**, *24*, 3173.
(56) Krupke, R.; Hennrich, F.; Weber, H. B.; Kappes, M. M.; Löhneysen, H. v. *Nano Lett.* **2003**, *3*, 1019.
(57) Li, J.; Qing, Z.; Yang, D.; Tian, J. *Carbon* **2004**, *42*, 2263.
(58) Li, P.; Xue, W. *Nanoscale Res. Lett.* **2010**, *5*, 1072.
(59) Schmidt, G.; Gallon, S.; Esnouf, S.; Bourgoin, J.-P.; Chenevier, P. *Chem.−Eur. J.* **2009**, *15*, 2101.
(60) Rehorek, A.; Plum, A. *Anal. Bioanal. Chem.* **2007**, *388*, 1653.
(61) Stasko, A.; Erentova, K.; Rapta, P.; Nuyken, O.; Voit, B. *Magn. Reson. Chem.* **1998**, *36*, 13.
(62) Lu, J.; Nagase, S.; Zhang, X. W.; Wang, D.; Ni, M.; Maeda, Y.; Wakahara, T.; Nakahodo, T.; Tsuchiya, T.; Akasaka, T.; Gao, Z. X.; Yu, D. P.; Ye, H. Q.; Mei, W. N.; Zhou, Y. S. *J. Am. Chem. Soc.* **2006**, *128*, 5114.
(63) Sortino, S.; Scaiano, J. C. *Photochem. Photobiol.* **1999**, *70*, 590.
(64) Berberidou, C.; Poulios, I.; Xekoukoulotakis, N. P.; Mantzavinos, D. *Appl. Catal. B: Environ.* **2007**, *74*, 63.
(65) Sedo, O.; Alberti, M.; Janca, J.; Havel, J. *Carbon* **2006**, *44*, 840.
(66) Xu, S.; Li, Y.; Zou, H.; Qiu, J.; Guo, Z.; Guo, B. *Anal. Chem.* **2003**, *75*, 6191.
(67) Okpalugo, T. I. T.; Papakonstantinou, P.; Murphy, H.; McLaughlin, J.; Brown, N. M. D. *Carbon* **2005**, *43*, 153.
(68) Stylidi, M.; Kondarides, D. I.; Verykios, X. E. *Appl. Catal., B* **2003**, *40*, 271.
(69) Liu, H.; Nishide, D.; Tanaka, T.; Kataura, H. *Nat. Commun.* **2011**, *2*, 309.
(70) Kim, W.-J.; Lee, C. Y.; O'Brien, K. P.; Plombon, J. J.; Blackwell, J. M.; Strano, M. S. *J. Am. Chem. Soc.* **2009**, *131*, 3128.
(71) Sarker, B. K.; Shekhar, S.; Khondaker, S. I. *ACS Nano* **2011**, *5*, 6297.
(72) Kim, W.; Javey, A.; Vermesh, O.; Wang, Q.; Li, Y.; Dai, H. *Nano Lett.* **2003**, *3*, 193.
(73) Lee, J. S.; Ryu, S.; Yoo, K.; Choi, I. S.; Yun, W. S.; Kim, J. *J. Phys. Chem. C* **2007**, *111*, 12504.
(74) Jeong, M. S.; Byeon, C. C.; Cha, O. H.; Jeong, H.; Han, J. H.; Choi, Y. C.; An, K. H.; Oh, K. H.; Kim, K. K.; Lee, Y. H. *Nano* **2008**, *3*, 101.
(75) Landi, B. J.; Ruf, H. J.; Evans, C. M.; Cress, C. D.; Raffaelle, R. P. *J. Phys. Chem. B* **2005**, *109*, 9952.
(76) Martel, R.; Schmidt, T.; Shea, H. R.; Hertel, T.; Avouris, P. *Appl. Phys. Lett.* **1998**, *73*, 2447.
(77) Perdew, J. P.; Burke, K.; Ernzerhof, M. *Phys. Rev. Lett.* **1996**, *77*, 3865.
(78) Kresse, G.; Furthmuller, J. *Phys. Rev. B* **1996**, *54*, 11169.
(79) Kresse, G.; Furthmuller, J. *Comput. Mater. Sci.* **1996**, *6*, 15.
(80) Kresse, G.; Hafner, J. *Phys. Rev. B* **1993**, *48*, 13115.